Available online at www.sciencedirect.com
SCIENCE DIRECT®
Biomaterials 25 (2004) 3463–3471
Biomaterials
www.elsevier.com/locate/biomaterials

Thermal sprayed hydroxyapatite splats: nanostructures, pore formation mechanisms and TEM characterization

H. Li[a], K.A. Khor[a,*], P. Cheang[b]

[a] School of Mechanical and Production Engineering, Advanced Materials Research Center (AMRC), Nanyang Technological University, 50 Nanyang Avenue, Singapore 639798, Singapore

[b] School of Materials Engineering, Advanced Materials Research Center (AMRC), Nanyang Technological University, 50 Nanyang Avenue, Singapore 639798, Singapore

Received 12 May 2003; accepted 10 October 2003

Abstract

Microstructure of thermal sprayed hydroxyapatite (HA) splats was characterized using transmission electron microscopy (TEM), and the formation mechanisms of micropores within the splats were investigated with the aid of simulated body fluids (SBF). High-velocity oxy-fuel and direct current (DC) plasma spray techniques were both utilized for the splats' deposition. The microstructure features of individual HA splats were revealed through TEM observation of as-sprayed, and ion-milled splats. Amorphous calcium phosphate and tricalcium phosphate phases were observed at the splats' fringes, which indicated that extensive decomposition of HA had occurred at these locations. The fringes of the HA splats are essentially nanostructured (~20–50 nm grains), while calcium phosphate grains up to 5 μm, depending on flattening state, are present at the center of the splats. Morphological observation classified the pores within the HA splats into three main categories according to distinctive features in their microstructure: open pores, sealed pores and through-thickness pores. It was found that particle velocity with which the particle impinged on the substrate surface, particle melt state, and structure of starting particle (mainly porosity) are the key variables in determining the formation and morphology of the micropores within the flattened splats. Influence of subsequent splats on the pores of prior deposited splat was also studied using an in vitro incubation test in SBF. Obvious pore-sealing action on the open pores was revealed, which was achieved through liquid filling of subsequent droplets. It was postulated that the overall porosity of a bulk coating could be attributed primarily to the sealed pores and flaws among the splats, and, it could be adequately governed through appropriate particle melt state and optimized velocity of the particles during coating formation.

Keywords: Transmission electron microscopy; Microstructure; Micropores; Thermal spray; Splat; Hydroxyapatite; Formation mechanism

1. Introduction

Thermal sprayed coatings have been extensively utilized in a wide variety of industries owing to their versatility and relative economy. Due to the anomalous inhomogeneous-layered structure, the coatings show a significant dependence of their mechanical performances on the microstructure. In order to enhance the properties of the coatings, structure improvement is the preferable approach. It is well known that the coatings actually exhibit an accumulated layered structure, which is composed of individual splats. Besides the contribution of the flaws, e.g. pores, cracks and among splats, microstructure of individual splats mainly accounts for the apparent structure of the bulk coating. The microstructure characterization of a single splat is essentially fundamental for a good understanding of thermal sprayed coatings. To date, some interesting results have been reported on microstructure of thermal sprayed splats [1–3]. In order to reveal detailed microstructure features in a single splat, transmission-electron microscopy (TEM) must be adequately involved for the characterization. Using a special polishing tool for their sample preparation, Chraska et al. reported the TEM observations on cross-sections of plasma sprayed zirconia splats [4,5], which revealed columnar grain growth within the splats. Unfortunately, due to the significant difficulty in TEM splat sample

*Corresponding author. Tel.: +65-6-790-5526; fax: +65-6-791-1859.
E-mail address: mkakhor@ntu.edu.sg (K.A. Khor).

0142-9612/$ - see front matter © 2003 Elsevier Ltd. All rights reserved.
doi:10.1016/j.biomaterials.2003.10.051

preparation, the understanding on the microstructure of splats is still incomplete.

Among the structure variables, which are responsible mainly for the mechanical properties, micropores play an important role [6–8]. The micropores within the thermal sprayed coatings have significant effect on their mechanical properties, e.g. Young's modulus [6], fracture toughness [9], etc. The random existence of the pores within a coating was believed to be one of the main factors responsible for the anisotropy in mechanical performances of the coating [6]. To date, increasing studies on formation mechanism of splats have been conducted [10–12]. Additionally, numerous constructive experimental investigations on the splat formation, mainly on clarification of relationships between splat morphology and spray parameters including substrate state (roughness, temperature, etc) [11,13], have shed insight into this topic. Meanwhile, useful attempts have been made in recent years towards theoretical understanding of the impact behavior of the individual splats during thermal spray [10,12,14] even though the assumptions for the simulations more or less restricted their valid applications. However, to date, the formation mechanism of the micropores during coating formation is still not clear, and the knowledge on pore formation is still lacking. A good understanding of such aspect is meaningful in a sense that improvement of the coating microstructure is possible through a cogent elucidation on the fundamental splat deposition process, and the formation of pores therein. In the present study, thermal sprayed hydroxyapatite (HA) splats were characterized using TEM from their intact surfaces and the formation mechanism of the micropores within the splats was studied through a splat morphology observation. In order to get different microstructures, both plasma spray and high-velocity oxy-fuel (HVOF) were utilized for the splat preparation on polished Ti–6Al–4 V substrates.

2. Experimental materials and setup

The starting HA powders were made through a wet chemical method and subsequently processed by spray drying to obtain near-spherical shape [15]. An additional annealing heat treatment at 900°C for 1.5 h was conducted to achieve an entirely crystalline structure. The powder size range was +45–75 μm, as determined through a laser particle size analyzer (Analysette 22, Fritsch Gmbh, Germany). Typical cross-sectional morphology of the HA powders used in the present study is shown in Fig. 1. A porous structure with the micropores of 1–2 μm in diameter is observed on metallographically polished cross-sections of spray-dried HA in a scanning electron microscope (SEM). Commercial titanium alloy Ti–6Al–4 V that measured $10 \times 10 \times 2\,mm^3$ in length, width, and thickness, respectively, was used as the substrate. Polishing was carried out on the substrate surface using 1 μm diamond paste before splats deposition. In order to get ready-for-observation splats for TEM surface characterization, the HA droplets (prepared by plasma spray in the present study) was directly sprayed onto copper slits (3.05 mm in diameter, 200 square mesh), which can be directly utilized for TEM observation. The copper slits were attached intimately on the polished Ti–6Al–4 V plates. The HA splats used for pore formation analysis were collected on polished Ti–6Al–4 V plate during the HVOF and plasma spray.

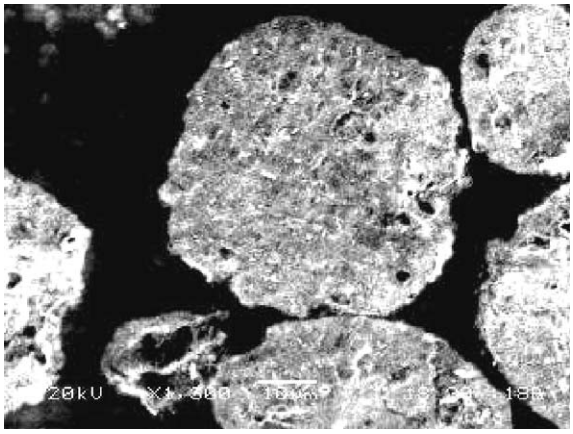

Fig. 1. Cross-sectional morphology of typical spray-dried HA particles showing a porous structure.

For the splats collection, a shielding plate was placed between the substrate and the spray stream to filter-off individual HA splats and, several holes of 1 mm in diameter were drilled on the plate. HV2000 HVOF system (Praxair Thermal Spray Inc, USA) with a nozzle diameter of 19 mm was used in the present study. Hydrogen was utilized as the fuel gas combusted in purified oxygen gas and the powder carrier gas was argon. A 40 kW DC plasma spray system (SG-100, Praxair Thermal Spray Inc, USA) was also employed in the present study to accomplish the splats preparation. The primary gas and powder carrier gas was argon. Helium was used as an auxiliary gas. The spray parameters of the HVOF and plasma spray are tabulated in Table 1.

The microstructure of the splats was analyzed using SEM (JEOL JSM-5600LV) and TEM (JEOL, JEM-2010) operated at 200 kV. In vitro incubation test was also conducted with an aim to reveal the influence of subsequent splats on the pores of prior deposited splats. Detailed description of the in vitro behavior has been provided in an earlier paper [16]. Due to the characteristic phase transformation of HA during coating formation to tricalcium phosphate (TCP), tetra-calcium phosphate (TTCP), CaO, or even amorphous calcium phosphate (ACP) [17–19], full dissolution of the

Table 1
Spray parameters of HVOF and plasma spray

HVOF	Plasma spray
Flow of H_2: 566 l/min	Net energy: 12 kW
Flow of O_2: 283 l/min	Flow of Ar: 31 l/min
Spray distance: 250 mm	Flow of He: 23 l/min
Flow of Ar (powder carrier gas): 19 l/min	Spray distance: 120 mm
Powder feeding rate: 8 g/min	Flow of Ar (powder carrier gas): 7 l/min
	Powder feeding rate: 8 g/min

Table 2
Composition of the SBF solution [20]

Ion	Ion concentration (mM) (SBF)
Na^+	142.0
K^+	5.0
Mg^{2+}	1.5
Ca^{2+}	2.5
Cl^-	147.8
HCO_3^-	4.2
HPO_4^{2-}	1.0
SO_4^{2-}	0.5

subsequent splat is possible through controlling the dissolution/precipitation procedures during the test. The ion concentrations of the simulated body fluid (SBF, pH = 7.40 [20]) are tabulated in Table 2. The in vitro test was conducted in a continuously stirred bath containing distilled water with a stable temperature of 37°C. The sample with calcium phosphate splats was incubated in 70 ml SBF contained in a polyethylene bottle. Once the sample was taken out from the solution, it was subsequently washed in distilled water, and then dried.

3. Results and discussion

Small pores are observed from the surface of the splats prepared by both HVOF and plasma spray techniques. Typical views under SEM are shown in Fig. 2. The size of the pores is revealed to be approximately 1–2 μm. Furthermore, large open pores were also discovered from different splats made from the HA particles, which are shown in Fig. 3. Through-thickness pores are also common within the splats (Fig. 4). Fig. 5 shows the evidence of the existence of an unrealized pore (defined here as sealed pore) within the plasma sprayed HA splats, which could be in correspondence to balanced gas-escaping and solidification rates. It is noted that such sealed pores were only present within plasma sprayed HA splats. Typical microstructure of HVOF sprayed HA splat is shown in Fig. 6. A

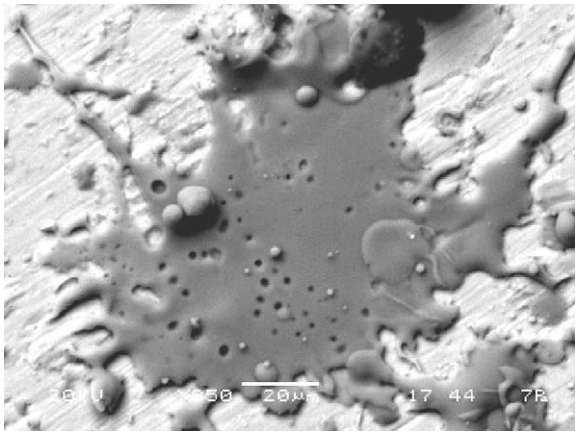

Fig. 2. A typical HA splat showing many small pores with a size of 1–2 μm.

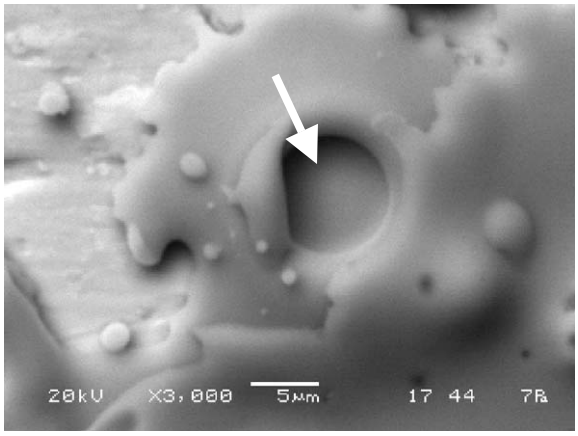

Fig. 3. A typical HA splat showing a large open pore with a size of 7–10 μm.

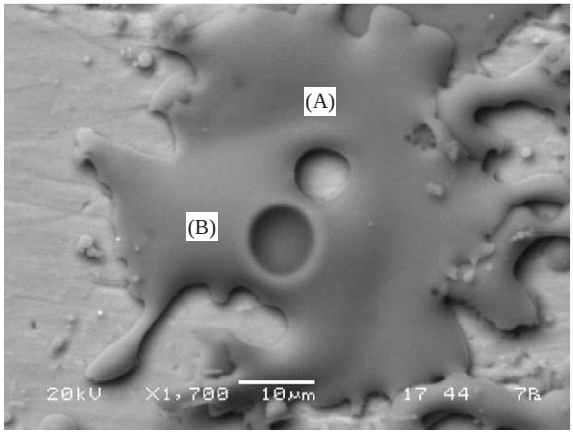

Fig. 4. A typical HA splat showing a through-thickness pore with a size of ~7 μm, together with an open pore.

partial-melt state of the particle and open pores within the splat are revealed.

It is noted that for the starting HA particles, a porous structure was demonstrated (Fig. 1). During plasma

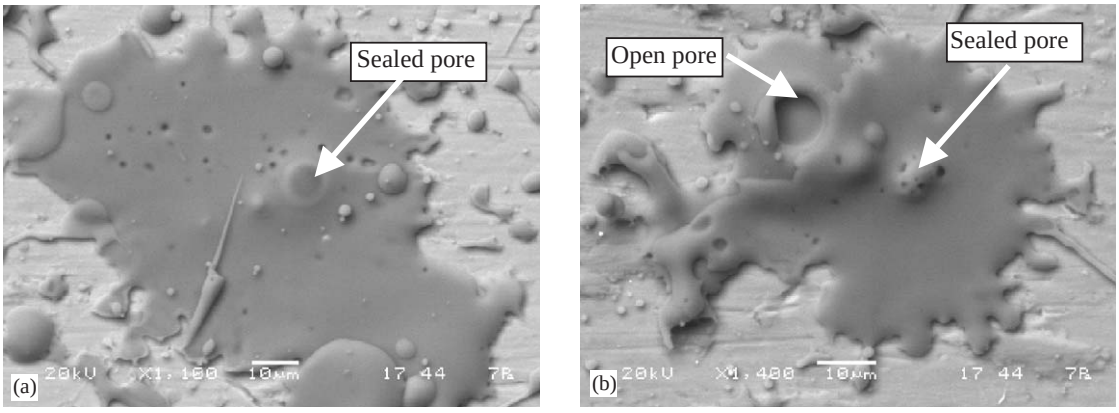

Fig. 5. Typical plasma sprayed HA splats showing existence of a sealed pore within the splat (a) and coexistence of a large open pore with the sealed pore (b).

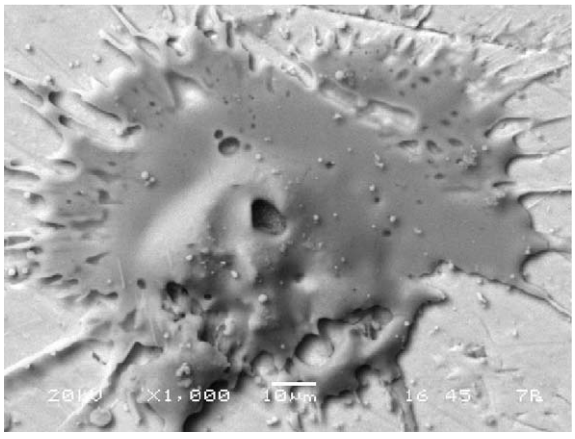

Fig. 6. Typical HVOF sprayed HA splat showing a partial-melt state and open pores within the splat.

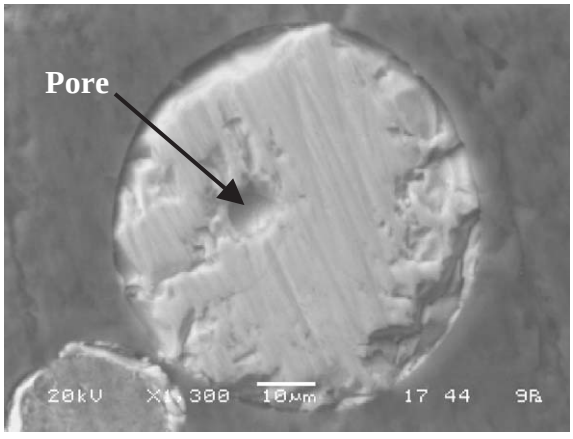

Fig. 7. Typical cross-sectional microstructure of a plasma sprayed HA particle showing the buildup of pre-existed micropores to be a large pore ($\sim 7\,\mu m$).

spraying of the HA powders, the particles were assumed to be fully melted, which can be deduced from the complete flattening of the splats. The small micropores ($<2\,\mu m$) are believed to exist as isolated pores within the starting particles. According to the dynamics of gas bubble within liquid [21], small gas bubbles would coalesce to form a large bubble within the droplet. That could be the reason why large pores were present within the splats (Figs. 3, 4 and 6). Analysis on plasma sprayed HA particles confirmed the clustering of the micropores during in-flight, which is typically shown in Fig. 7. The particles were collected through plasma spraying the HA powders into distilled water using identical spray parameters. It shows that, compared to the starting particles (Fig. 1), a dense cross-sectional microstructure is evident within the sprayed particle. The large pore ($\sim 7\,\mu m$) is likely the result of the buildup of the pre-existed micropores. Statistical observation on plasma sprayed particles revealed different locations of the large pores within the particles. The formation of sealed pores was likely to be the result of a rate balance between gas bubble escaping and particle solidification. Under the same spray conditions, formation of either open pores or through-thickness pores could be attributed to the locations of the original gas bubbles. Partial-melt state of the HA particles during HVOF spraying could be responsible in part for the difference in pore morphology within a splat from that deposited by plasma spray. An earlier study on assessing the significance of the meltstate of HVOF sprayed HA revealed that, typically, the melt fraction in the particles ranged from 20% to over 90% depending on the starting particle size. Particles around $20\,\mu m$ would likely to be over 80% melted. Therefore, apart from porosity of starting powders, the melt state of the particles during spraying is an important factor influencing the final pore structure of bulk coating. Furthermore, due to the high velocity ($>400\,m/s$) attained by the particles during HVOF spray, some splats were even completely disintegrated after impinging on the substrate, which is shown in Fig. 8. On the other hand, plasma sprayed particles have velocities well below $80\,m/s$. It can therefore be concluded that particle velocity with which the particle impinges on the substrate plays an exceedingly important role in determining the pore structure

and hence, overall porosity of the accumulated bulk coating. The increase in initial droplet velocity has been numerically proven to be useful in enhancing the flattening extent of droplet [22], which would result in different types of pores.

It should be noted that for the first layer of the coating (the splat in this case), since thermal conductivity of the Ti–6Al–4 V is higher than HA, a high solidification rate would be a result (typically $\sim 10^6$ K/s). The high solidification rate obviously influences the pore morphology, that is, more sealed pores within the first layer and smaller pore size than those subsequently deposited layers would be expected. Even though due to the rapid solidification at the interface between the splat and substrate, a porous microstructure was claimed at the bottom surface of a metallic splat on the room temperature substrate [23], the present experimental observation did not give evidence of such phenomenon.

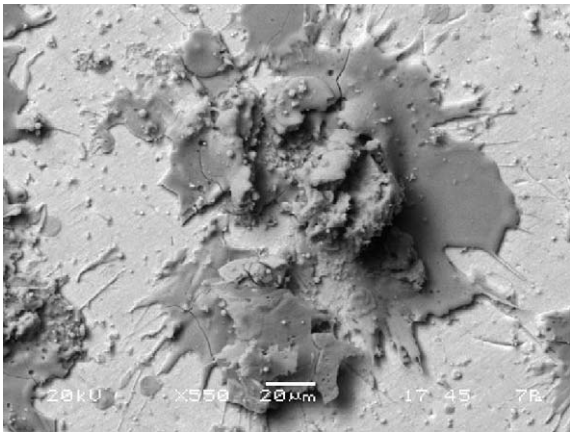

Fig. 8. A typical HVOF HA splat showing a destroyed morphology caused by the high velocity and partial-melt state of the particle upon the impingement.

The subsequent droplet (or partially melted particle) could have remarkable influence on the open pores as exhibited by the former splat due to the considerably high velocity of the droplet. Typical morphology changes of the folded splats induced by the in vitro incubation for 1.5 h are shown in Fig. 9. A trace of liquid filling from the subsequent droplet is revealed. The folded splat shows significant re-sealing effect on the micro pores of the former splat formed. It has been pointed out that the phases brought about by the HA transformation have marked dissolvability in the SBF [24]. It is clear that the injected part is composed mainly of dissolvable (bio-resorbable) phases, such as TTCP,

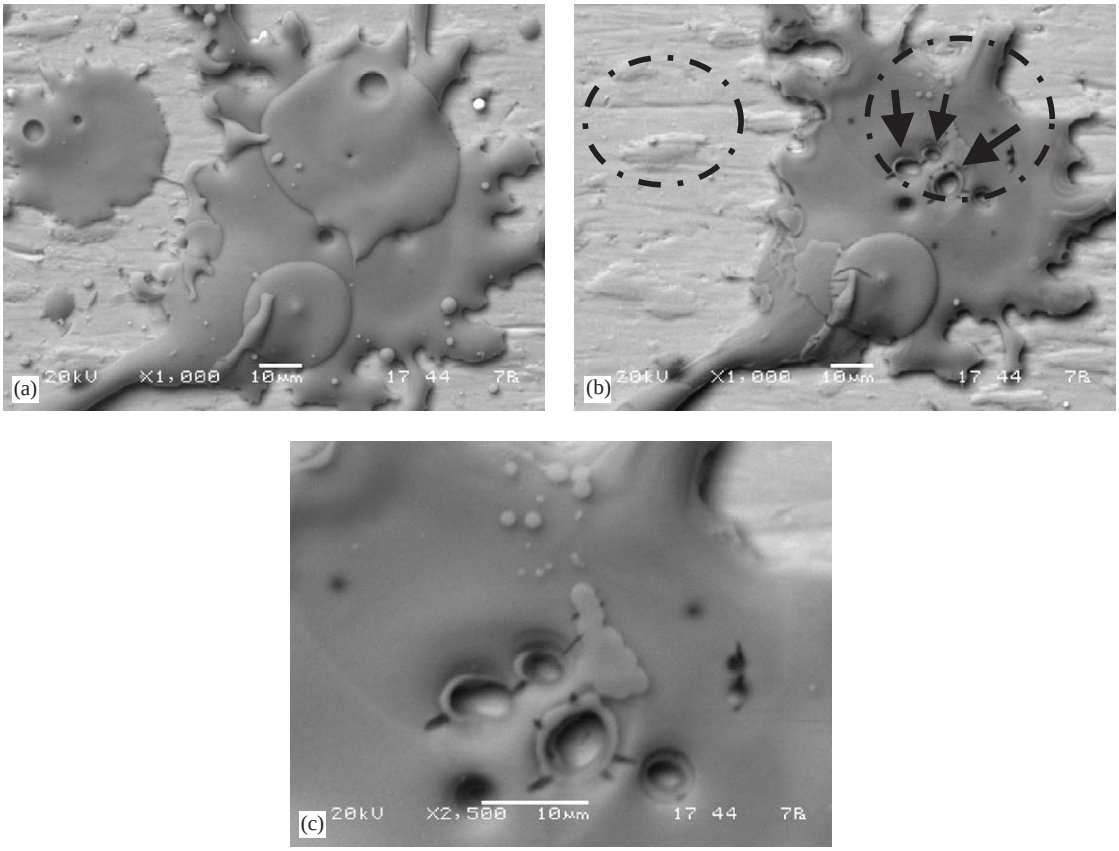

Fig. 9. Microstructure changes of folded HA splats after 1.5 h incubation in vitro showing a healing effect of subsequent splat on the open pores of former splat, (a) before the incubation, (b) after the incubation, the subsequent splat dissolved into the SBF entirely, and (c) under higher magnification of image (b).

TCP, ACP, etc. and in a previous report, it has been claimed that phase transformation of HA took place mainly within the melted part of the particle [19]. Liquid with high impingement speed can be spilled into the open (through-thickness) pores easily, and hence, decreases the porosity of resultant coating. It is therefore acknowledged that particle velocity is crucial as it directly governs the impact, with which the particle impinges on the former splat to affect pore healing (sealing). This could at least be the partial reason why HVOF coatings are typically denser than plasma sprayed coatings, given that powder feedstock and powder feed-rate are similar. The filling of the liquid materials into the micropores can also be suitably explained by the large impingement pressure brought about by the subsequent splat, which has been described in an earlier report [25]. It should be noted that only liquid could achieve such improvement. With regard to the healing effect, it can be concluded that only the sealed pores and the unbonded areas among splats contribute predominately to the overall porosity of a bulk coating. Melt state and velocity of the sprayed particles during spray may play the most important role in determining the overall porosity through their influence on pore structure.

The formation of the micropores, open pores or sealed pores, caused by steady flow of the gas within a droplet could be explained using dynamics of a spherical bubble within liquid, provided that the particles were fully melted during the spray process. It is postulated that when the droplet impinges the substrate, the dissolved gas within the droplet is subjected to sudden decompression, and squeezing out of the gas is in response to the formation of open pores. The depiction of a pore within a droplet is shown in Fig. 10. Suppose inside the bubble the gas pressure p_b changes with time according to some known law, then the bubble radius R (supposed to always be in spherical shape) is also a function of time [21]. As the fluid pressure (p_{at}) starts to increase (first stage of the impingement in this case), the bubble soon shrinks and collapses. When the radius of the gas bubble becomes zero (full release of the gas to form open pores), the following formula [21] can be used to get the open pore formation time by neglecting the influence of viscosity, bubble pressure change and surface tension:

$$t_0 = 0.915 R_m \left(\frac{\rho}{p_{at} - p_b} \right)^{1/2}, \quad (1)$$

where t_0 is the time as the gas bubble is squeezed out in the present case (open pore formation duration), R_m is the maximum gas bubble diameter within the droplet, ρ is the density of the liquid particle, p_{at} is the pressure imparted from the surrounding liquid on the bubble as shown in Fig. 9 and p_b is the pressure of the gas bubble. It is obvious that during the flattening stage, p_{at} changes significantly. Since the solidification time of a droplet is limited, from the equation, it is clear that small open pores can be more easily formed than larger ones due to the time required.

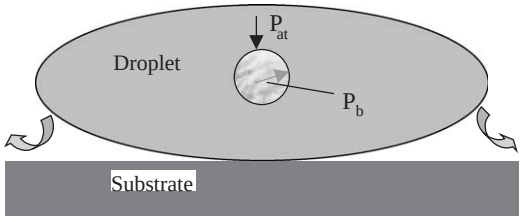

Fig. 10. Depiction of a gas bubble within a droplet upon impingement on the substrate surface.

The final size of the sealed pores is likely to be significantly influenced by the solidification rate. It is well known that HVOF sprayed particles have higher velocity, hence higher p_{at} than plasma sprayed particles. This can explain why the sealed pores were absent in HVOF sprayed HA splats, that is, before the sealed pore formation, the gas has already escaped to form an open pore. After complete solidification, the final compressed micropores would be responsible, at least partially, for the flaws formed after coating deposition, such as the formation of microcracks, etc. which were a result of release of the internal gas pressure within the entrapped pores. It is reasonable to assume that if the solidification rates of the liquid splat were very fast (which is $\sim 10^6$ K/s for plasma spray), the unreleased pores would have a pressure higher than that of the atmosphere.

It should be noted that after complete solidification, the high pressure within the sealed pores could be released through formation of other flaws, such as microcracks, fragmentation and residual stresses, which have been revealed to be significantly influenced by substrate temperature rather than particle velocity and temperature [26]. With regard to the formation mechanism of the residual stresses within a splat that arose predominantly from quenching stresses and thermal stresses [27], the present results can adequately explain those findings that the substrate temperature exhibits marked influence on the rate ratio of gas escaping to solidification. This in turn is responsible for varied pore structures. Furthermore, due to the lower coefficient of thermal expansion of the Ti–6Al–4 V (9.0×10^{-6}/K) than HA (16.0×10^{-6}/K [28]), a residual tensile stress would be present within the splats. This would influence the crack formation within the splat during the final stage of solidification. The duration of different stages were influenced by the droplet parameters, e.g. velocity, diameter, overall profile, and heat transfer between the splat and substrate [29,30].

Even though many assumptions were made, previous simulation work still gave some interesting results on the flattening behavior of the splats. It has been

theoretically shown that with increasing initial droplet velocity, the final total freezing time effectively decreased [22,25]. This could account for the phenomenon revealed in HVOF and plasma sprayed coatings that droplet velocity would influence release of entrapped gas within the exceedingly short time prior to complete solidification. It should be noted that the present study only investigated the splats formed on the substrates without preheating. Previous investigations have shown important influence of substrate temperature on the morphology of the splats [23].

The topographical morphology of the plasma sprayed HA splats (Figs. 2, 4 and 5) have shown their graphical features, surrounding fringes, which resulted mainly from the splashing during splat formation and thick central portion. It is not surprising that, for the splats, the center is the thickest part within the splat owing to the unique flattening behavior of thermal sprayed splats. ACP phase is detected at the fringes of the intact as collected individual HA splats observed under TEM (Fig. 11). Furthermore, the structure with folded nanosized grains ($\sim$30 nm) at the splat fringes is disclosed (Fig. 12). The folding state is likely due to the flattening of the droplet together with simultaneous solidification. Apart from the appearance of ACP at the fringes of the plasma sprayed HA splats, α-,β-TCP is also revealed, which is shown in Fig. 13. In order to further reveal the microstructure of the parts near to the center of the HA splats, ion milling of the samples was conducted. Enlarged grains (>400 nm) were revealed within the parts near to the center of the HA splats compared to their fringes (Fig. 14). Unfortunately, due to the random ion milling on the splats, it was difficult to state exactly which part of the splat was observed under the TEM.

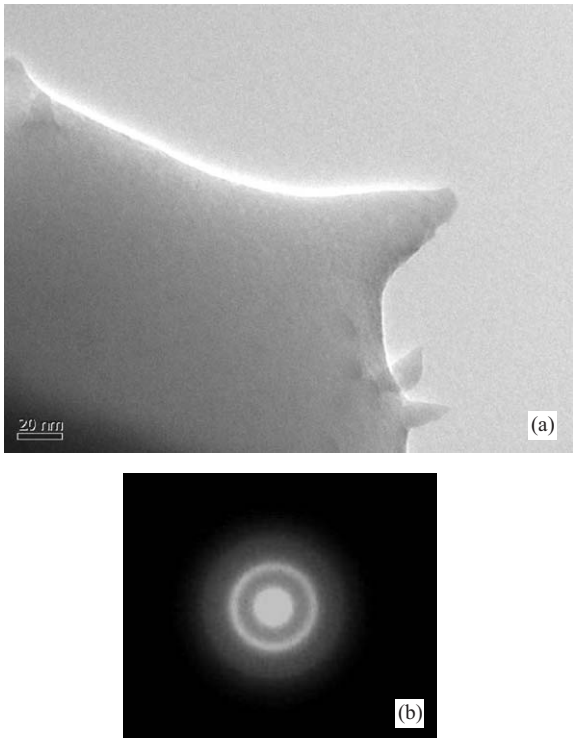

Fig. 11. TEM morphology of an individual HA splat at its fringe (a) showing a typical amorphous structure suggested by its diffraction pattern detected at selected area (b).

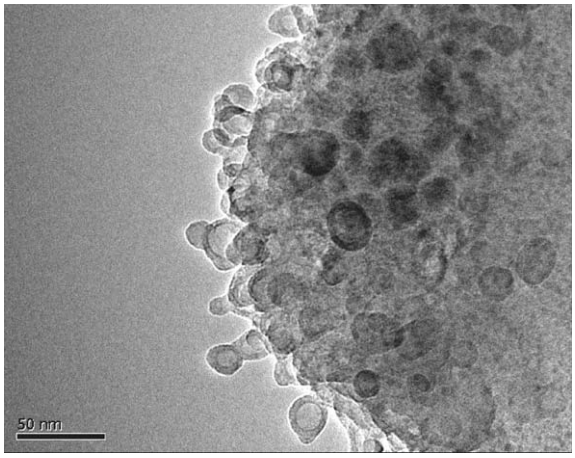

Fig. 12. TEM morphology of a single HA splat at its fringe showing a typical folded grains induced by the droplet flattening.

Fig. 15 shows the SEM view of single plasma sprayed HA splat at its center. The grain size within this part can be up to 5 μm ($\sim$1 μm–$\leqslant$5 μm) depending on flattening state of the splats. Compared to its fringes (Figs. 12–14), the increase in the grain sizes of the splats is significant. The accumulated coating, hence, must have a mixed nano- and micro-structure. Enhanced cooling of substrate during coating deposition could effectively increase the content of the nanosized grains within the HA coatings.

4. Conclusions

Pore formation mechanism within thermal sprayed HA splats was discussed on the basis of revealed features through SEM, TEM, and in-vitro evaluation. The micropores within a HA splat made from porous starting particles are predominantly divided into three categories in accordance to their apparent morphology and sizes: open pores (small pores, <2 μm in diameter, and large pores), through-thickness pores and sealed pores. The open pores and the subsequently flattened droplet through liquid filling was found to effectively 'seal' through-thickness pores within a splat. The sealed pores together with characteristic flaws among the splats are likely to contribute cogently to the porosity of the resultant coating, which is formed through the accumulation of splats. It is postulated that adequate particle velocity and a sufficiently apt melt state of the sprayed

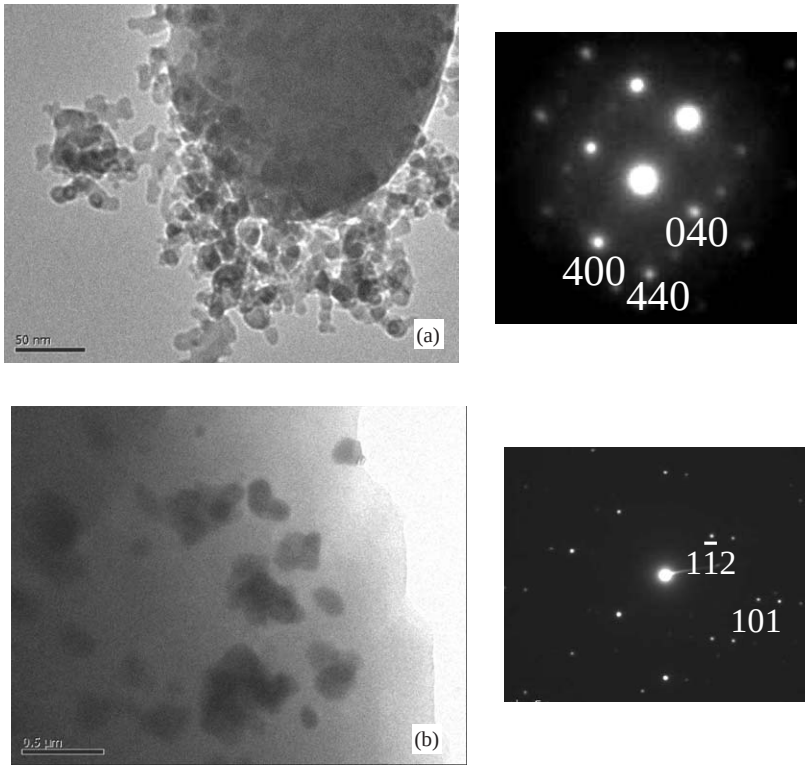

Fig. 13. TEM microstructure of a single HA splat at its fringe showing presence of (a) α-TCP indicated by the selected diffraction pattern from its [0 0 1] zone axis, and (b) β-TCP indicated by the selected diffraction pattern from its [$\bar{1}$ 1 1] zone axis.

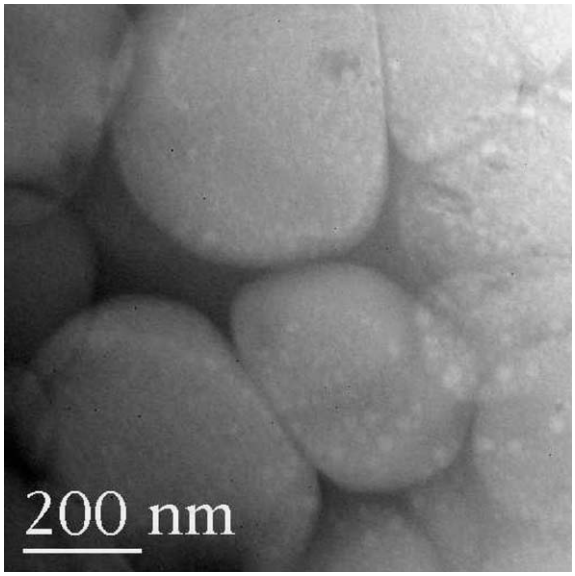

Fig. 14. TEM microstructure of a single HA splat at the part near to its center showing an increased grain size compared to those grains located at the fringes.

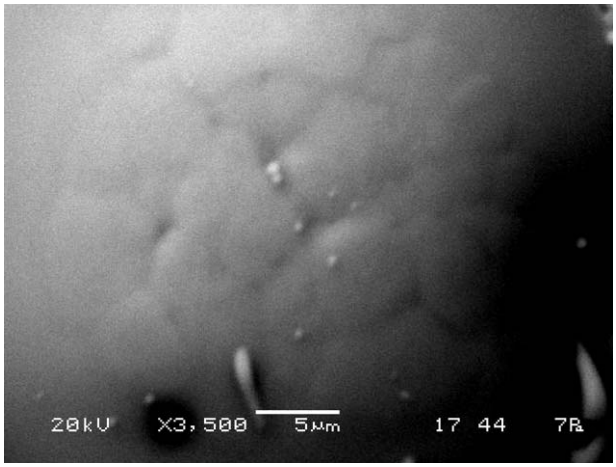

Fig. 15. SEM topographical microstructure of a single HA splat at its center showing a grain size of ~5 mm.

particles upon impingement is beneficial towards attaining a low-porosity level. The present results indicated that the flattening and solidification of the droplet upon its impingement on the substrate occurred simultaneously. Furthermore, plasma sprayed HA splats were characterized using TEM and, revealed nano-sized calcium phosphate grains (~30 nm) at the intact splats' fringes. Significant phase transformation of HA at splats' surrounding parts was confirmed. It was also found that the grains at the fringes have the smallest size, while those located at the splats' center have the largest dimension (up to 5 μm).

References

[1] Pasandideh-Fard M, Pershin V, Chandra S, Mostaghimi J. Splat shapes in a thermal spray coating process: simulations and experiments. J Therm Spray Technol 2002;11:206–17.

[2] Delplanque JP, Cai WD, Rangel RH, Lavernia EJ. Spray atomization and deposition of tantalum alloys. Acta Mater 1997; 45:5233–43.

[3] Jiang X, Sampath S, Herman H. Grain morphology of molybdenum splats plasma-sprayed on glass substrates. Mater Sci Eng 2001;A299:235–40.

[4] Chraska T, King AH. Transmission electron microscopy study of rapid solidification of plasma sprayed zirconia—Part I. First splat solidification. Thin Solid Films 2001;397:30–9.

[5] Chraska T, King AH. Effect of different substrate conditions upon interface with plasma sprayed zirconia—a TEM study. Surf Coat Technol 2002;157:238–46.

[6] Sevostianov I, Kachanov M. Modeling of the anisotropic elastic properties of plasma-sprayed coatings in relation to their microstructure. Acta Mater 2000;48:1361–70.

[7] Leigh SH, Lin CK, Berndt CC. Elastic response of thermal spray deposits under indentation tests. J Am Ceram Soc 1997;80: 2093–9.

[8] Li CJ, Ohmori A, McPherson R. Relationship between microstructure and Young's modulus of thermally sprayed ceramic coatings. J Mater Sci 1997;32:997–1004.

[9] Callus PJ, Berndt CC. Relationships between the mode II fracture toughness and microstructure of thermal spray coatings. Surf Coat Technol 1999;114:114–28.

[10] Pasandideh-Fard M, Pershin V, Chandra S, Mostaghimi J. Splat Shapes in a thermal spray coating process: simulations and experiments. J Therm Spray Technol 2002;11:206–17.

[11] Sampath S, Jiang X. Splat formation and microstructure development during plasma spraying: deposition temperature effects. Mater Sci Eng 2001;A304–306:144–50.

[12] Gougeon P, Moreau C. Simultaneous independent measurement of splat diameter and cooling time during impact on a substrate of plasma-sprayed molybdenum particles. J Therm Spray Technol 2001;10:76–82.

[13] Montavon G, Sampath S, Berndt CC, Herman H, Coddet C. Effects of vacuum plasma spray processing parameters on splat morphology. J Therm Spray Technol 1995;4:67–74.

[14] Bertagnolli M, Marchese M, Jacucci G, Doltsinis ISt, Noelting S. Thermomechanical simulation of the splashing of ceramic droplets on a rigid substrate. J Comput Phys 1997;133: 205–21.

[15] Kweh SWK, Khor KA, Cheang P. Production and characterization of hydroxyapatite (HA) powders. J Mater Processing Technol 1999;89–90:373–7.

[16] Khor KA, Li H, Cheang P, Boey SY. In vitro behavior of HVOF sprayed calcium phosphate splats and coatings. Biomaterials 2003;24:723–35.

[17] Gross KA, Berndt CC. Thermal processing of hydroxyapatite for coating production. J Biomed Mater Res 1998;39:580–7.

[18] McPherson R, Gane N, Bastow TJ. Structural characterization of plasma-sprayed hydroxylapatite coatings. J Mater Sci: Mater Med 1995;6:327–34.

[19] Li H, Khor KA, Cheang P. Effect of the powders' melting state on the properties of HVOF sprayed hydroxyapatite coatings. Mater Sci Eng 2000;A293:71–80.

[20] Kokubo T, Kushitani H, Sakka S, Kitsugi T, Yamamuro T. Solutions able to reproduce in vivo surface changes in bioactive glass-ceramic A-W[3]. J Biomed Mater Res 1990;24:721–4.

[21] Zapryanov Z, Tabakova S. Dynamics of bubbles, drops and rigid particles. The Netherlands: Kluwer Academic Publishers; 1999.

[22] Liu H, Lavernia EJ, Rangel RH. Numerical simulation of substrate impact and freezing of droplets in plasma spray processes. J Phys D: Appl Phys 1993;26:1900–8.

[23] Fukumoto M, Nishioka E, Matsubara T. Flattening and solidification behavior of a metal droplet on a flat substrate surface held at various temperatures. Surf Coat Technol 1999; 120–121:131–7.

[24] Ducheyne P, Radin S, King L. The effect of calcium phosphate ceramic composition and structure on in vitro behavior, I. Dissolution. J Biomed Mater Res 1993;27:25–34.

[25] Li H, Khor KA, Cheang P. Impact formation and microstructure characterization of thermal sprayed hydroxyapatite/titania composite coatings. Biomaterials 2003;24:949–57.

[26] Matejicek J, Sampath S. Intrinsic residual stresses in single splats produced by thermal spray processes. Acta Mater 2001;49: 1993–9.

[27] Clyne TW, Gill SC. Residual stresses in thermal spray coatings and their effect on interfacial adhesion: a review of recent work. J Therm Spray Technol 1996;5:401–18.

[28] Fischer GR, Bardhan P, Geiger JE. Lattice thermal expansion of hydroxyapatite. J Mater Sci Lett 1983;2:577–8.

[29] Zhao Z, Poulikakos D, Fukai J. Heat transfer and fluid dynamics during the collision of a liquid droplet on a substrate—I. Modeling. Int J Heat Mass Transfer 1996;39:2771–89.

[30] Delplanque JP, Rangel RH. A comparison of models, numerical simulation, and experimental results in droplet deposition processes. Acta Mater 1998;46:4925–33.